Induced dipole dominant giant electrorheological fluid

Rong Shen(沈容), Kunquan Lu(陆坤权), Zhaohui Qiu(邱昭晖), and Xiaomin Xiong(熊小敏)

Citation: Chin. Phys. B, 2023, 32 (**7**): 078301. DOI: 10.1088/1674-1056/accd4e
Journal homepage: http://cpb.iphy.ac.cn; http://iopscience.iop.org/cpb

What follows is a list of articles you may be interested in

Electrostatic switch of magnetic core-shell in 0-3 type LSMO/PZT composite film

Bo Chen(陈波), Zi-Run Li(李滋润), Chuan-Fu Huang(黄传甫), Yong-Mei Zhang(张永梅)
Chin. Phys. B, 2020, 29 (**9**): 097702. DOI: 10.1088/1674-1056/abab73

Recent advances, perspectives, and challenges inferroelectric synapses

Bo-Bo Tian(田博博), Ni Zhong(钟妮), Chun-Gang Duan(段纯刚)
Chin. Phys. B, 2020, 29 (**9**): 097701. DOI: 10.1088/1674-1056/aba603

The electric field and frequency responses of giant electrorheological fluids

Hanqing Zhao(赵汉青), Rong Shen(沈容), Kunquan Lu(陆坤权)
Chin. Phys. B, 2018, 27 (**7**): 078301. DOI: 10.1088/1674-1056/27/7/078301

Electrical field-driven ripening profiles of colloidal suspensions

Zi-Rui Wang(王子瑞), Wei-Jia Wen(温维佳), Li-Yu Liu(刘雳宇)
Chin. Phys. B, 2018, 27 (**6**): 068301. DOI: 10.1088/1674-1056/27/6/068301

First-principles study of the relaxor ferroelectricity of Ba(Zr, Ti)O_3

Yang Li-Juan (杨丽娟), Wu Ling-Zhi (武灵芝), Dong Shuai (董帅)
Chin. Phys. B, 2015, 24 (**12**): 127702. DOI: 10.1088/1674-1056/24/12/127702

Induced dipole dominant giant electrorheological fluid

Rong Shen(沈容)[1], Kunquan Lu(陆坤权)[1,†], Zhaohui Qiu(邱昭晖)[2], and Xiaomin Xiong(熊小敏)[2]

[1] *Beijing National Laboratory for Condensed Matter Physics, Key Laboratory of Soft Matter and Biological Physics, Institute of Physics, Chinese Academy of Sciences, Beijing* 100190, *China*

[2] *School of Physics, Sun Yat-sen University, Guangzhou* 510275, *China*

(Received 8 March 2023; revised manuscript received 22 March 2023; accepted manuscript online 16 April 2023)

Traditional dielectric electrorheological fluid (ER) is based on the interaction of dielectric particle polarization, and the yield stress is low, which cannot meet the application requirements. The giant ER (GER) effect is caused by orientations and interactions of polar molecules adsorbed on the particle surfaces. Despite the high yield stress, these polar molecules are prone to wear and fall off, resulting in a continuous reduction in shear stress of GER liquid, which is also not suitable for application. Here we introduce a new type of ER fluid called induced dipole dominant ER fluid (ID-ER), of which the particles contain oxygen vacancies or conductor microclusters both prepared by high energy ball milling (HEBM) technique. In the electric field E, oxygen vacancies or conductor microclusters form induced dipoles. Because the local electric field $E_{\rm loc}$ in the gaps between particles can be two to three orders of magnitude larger than E, the induced dipole moments must be large. The strong interactions of these induced dipoles make the yield stress of the ID-ER fluid reaching more than 100 kPa. Since there are oxygen vacancies or conductor microclusters everywhere in the particles, the particles will not lose the function due to surface wear during use. The experimental results show that the ID-ER fluid possesses the advantages of high shear stress, low current density, short response time, good temperature stability, long service life, and anti-settlement, *etc.* The comprehensive performance is much better than the existing ER materials, and also the preparation method is simple and easy to repeat, thus it should be a new generation of ER fluid suitable for practical applications.

Keywords: electrorheological fluid, induced dipole, vacancies, high energy ball milling

PACS: 83.80.Gv, 77.22.Ej, 61.72.jd, 81.20.Wk **DOI:** 10.1088/1674-1056/accd4e

1. Introduction

In 1949, Winslow[1] reported that the shear stress of a suspension composed of solid particles and insulating liquid would increase with the applied electric field, which was called the electrorheological (ER) effect. Because of the potential application prospect of this effect, great efforts have been made for the decades to obtain ER materials that can be used in practice. To date, however, ER fluids have still not been widely used in technology and engineering, due to no ER fluids with good enough comprehensive performance suitable for applications.

In the research history of ER fluids, it has mainly experienced the developments of two generations of ER fluid materials. The first generation, termed as dielectric ER fluids, was prepared by mixing solid dielectric particles with insulating oil, of which the effect is based on the interactions of dielectric particles polarized in the electric field.[2–5] Thus the yield stress τ_y must be proportional to the square of electric field E, *i.e.*, $\tau_y \propto E^2$. Despite extensive tests performed, the yield stress of the prepared ER fluids was only reach few kPa. In 1996, Ma *et al.* made a theoretical calculation using the first principles, and concluded that the upper bound of the yield stress of this kind of ER fluids could only reach about 10 kPa.[6] The mechanism of traditional ER fluid determines that its yield stress is low, which is unable to meet the applications requirements. In 1998, it was found that the ER fluid prepared by surface modified Sr–Ti–O particles possessed a high yield stress, reaching about 30 kPa at an electric field of 3 kV/mm.[7,8] In 2003, an ER fluid consisted of Ba–Ti–O nano-particles with urea polar molecules coated prepared by Wen *et al.* had a yield stress of over 100 kPa, which was called giant ER (GER) fluid.[9] For GER materials the solid particles are generally prepared by wet chemical methods, and their surfaces are coated with polar molecules.[10–14] As an electric field E is applied, the polarized particles attract and get close to each other, and the local electric field $E_{\rm loc}$ between the particles can be 10^2–10^3 times of E.[15–19] Such a high $E_{\rm loc}$ can cause the polar molecules on the particle surface in the region to orientate along $E_{\rm loc}$ and interact with the polarized units on the surfaces of adjacent particles. These interactions are much larger than that between of polarized particles as in dielectric ER fluid, thus results in high shear stress up to several hundred kPa in GER. Because of the effect of ER originated from the orientation of inherent dipole moment the relationship between yield stress and electric field should be linear, that is, $\tau_y \propto E$, which is different from that of $\tau_y \propto E^2$ as in conventional ER fluid. This GER is also known as polar molecule dominant ER fluids (PM-ER),[11,12] which can be considered as the second generation ER fluid with high yield stress. For the PM-ER fluids, however, the fatal flaw is that the coating or modification layer on the particle surface are easy to be worn and the polar molecules fail, result-

†Corresponding author. E-mail: lukq@iphy.ac.cn

ing in the continuous decline of its shear stress with wearing time. Although the wear resistance can be slightly improved by dissolving polar molecules into the liquid,[20,21] it is still not suitable for application because polar molecules will lose their polarity due to the actions such as space charge.

It can be seen from the above that the existing first-generation of the dielectric ER fluid and second-generation PM-ER fluid have not been widely used in practice so far due to their inherent deficiency. New ER fluids that can be applied in technology and engineering is eagerly anticipated.

In the study, we found that the ER fluids prepared with two kinds of modified dielectric particles provide excellent ER effect: One is to introduce a large number of vacancies into the dielectric particles; The other is to embed conductive microclusters in the dielectric particles. Due to the action of the high local field $E_{\rm loc}$ at particle spacing, the vacancies or the conductive microclusters on particle surfaces can generate large induced dipole moment and cause strong interactions between particles, resulting in the high shear stress of the ER fluids. This new ER fluid can be referred to as an induced dipole-dominanted ER (ID-ER) fluid.

Present paper reports the preparation method as well as the action principle for ID-ER fluids, which are different from that of the dielectric ER and PM-ER fluids. The particles in ID-ER fluids containing vacancies or conductive microclusters both are prepared by high-energy ball milling (HEBM) technique. The raw materials before HEBM are either pure dielectric particles or dielectric particles mixed with a small amount of conductive material. The obtained ID-ER fluids exhibit attractive comprehensive performance: high yield stress ($>$ 100 kPa), low current density ($<$ 20 μA/cm^2), nice temperature stability and wear resistance, settlement resistance as well. Furthermore, the preparation method is simple, good repeatability, low cost. Therefore, ID-ER fluids should be the new type of ER fluids suitable for applications.[22]

We have studied the TiO_2 particles containing oxygen vacancies treated by HEBM method as well as the properties of prepared ID-ER fluids with these particles, and will introduce the results in detail. The ID-ER fluids prepared with some other dielectric particles besides TiO_2 containing oxygen vacancies are briefly described as well. As for the ID-ER fluid consisted of the particles embedded with conductive microclusters, we have discussed the method and principle of preparing embedded carbon microclusters by heat treatment in previous article,[23] and the results for the particles processed by HEBM are supplemented briefly in this paper.

This article is presented in the following order: firstly, the preparation method of particles used in ID-ER fluid; the characterization of morphology, structure, and properties of the particles modified by HNBM; the property test of ID-ER fluid; finally, the proposed physical mechanism for explaining the ID-ER effect. In addition, the deficiency shortcoming of ID-ER fluid is pointed out.

2. Experimental details

Market-purchased oxide dielectric particles, such as TiO_2 powder, were used as the raw material and heated for several hours in a furnace above 400 °C to remove any possible adsorbents from the particles. The powder was then treated with HEBM and milled for more than 10 hours. On the other hand, by mixing small amount of graphite or metal powder to dielectric particles to perform HEBM, the particles with conductive microclusters embedded can be achieved. The longer ball milling time is beneficial to get sufficient oxygen vacancies for the prepared particles, or the particles with better conductive microcluster dispersion.

Particle density was measured by a true density instrument, x-ray diffraction (XRD), scanning electron microscopy (SEM), high resolution transmission electron microscope (HRTEM), electron paramagnetic resonance (EPR), and x-ray absorption fine structure (XAFS) technique were used to study and compare the morphologies and microstructures of particles before and after HEBM. Thus the oxygen vacancies and conductive microclusters in the particles induced by HEBM were detected and analyzed. XAFS was performed at Beijing Synchrotron Radiation Facility (BSRF).

The readied particles through HEBM were mixed with silicone oil or machine oil to prepare ID-ER fluid. Shear stress were measured by self-made flat plate rheometer or Anton Paar rheometer. The flat plate rheometer with the plates of rough surfaces can measure ER samples with shear stress up to more than 200 kPa. The yield stress was measured at a shear rate of 0.2 s^{-1}.

Response time and frequency dependence measurements for the ID-ER fluids at different shear rates were performed by using a home-made rotary rheometer connected to Trek 10/40A type frequency and waveform adjustable high voltage power supply. The change rate of the rising and falling edges of the square wave was 750 V/μs and the data acquisition rate was 1000 s^{-1} or 4000 s^{-1}.

For testing the abrasion resistance of ER fluid, the sample was sealed in a rotating container composed of an inner roller with diameter of 40.5 mm and an outer cylinder with diameter of 42 mm, which rotated for a long period with a shear rate of 300 s^{-1} without electric field applied. During the period the ID-ER samples were taken out several times to measure the changes of yield stress of them at E field due to the abrasion.

We mainly studied anatase type TiO_2 nano-particles treated by HEBM technique as well as the prepared ID-ER fluid. Other powders with high dielectric constant such as rutile-type TiO_2, $BaTiO_3$, $CaTiO_3$, $CaCu_3Ti_4O_{12}$ as well as

SiO_2 powders with lower dielectric constant were also processed by HEBM and the properties of ID-ER fluids prepared with these particles were investigated, respectively. In addition, several ID-ER fluids consisted of the particles with graphite or metal microclusters embedded were tested.

3. Results and discussion

3.1. Microstructure changes and oxygen vacancies in particles induced by HEBM

HEBM or saying mechanical alloying (MA) technique was developed in the 1970s to prepare composite materials. In the milling process, a large number of defects and microstructures are generated through intense mechanical actions such as collision, extrusion, shear and friction, which make the material undergo non-equilibrium transformation. Many new materials which are difficult to be obtained by other conventional methods can be synthesized.[24–27] HEBM studies on TiO_2 nanopowders have shown that anatase TiO_2 can be transformed into rutile structure,[28,29] and a large number of oxygen vacancies can be created.[30,31] The simulation results show that the vacancies increase with the milling time and gradually reach saturation.[32]

In our investigation, the initial particles were anatase-type TiO_2 with a diameter of about 20 nm–30 nm. The comparisons of observed results for TiO_2 powders before and after HEBM are given below. Figures 1 and 2 show STEM, HRTEM images, and x-ray diffraction spectra of TiO_2 samples before and after milling respectively. It can be seen that HEBM can cause the TiO_2 powder transformed from anatase structure to rutile phase dominated structure with a larger disorder and a small size about 10 nm–15 nm. The density measurements show that the initial density of anatase-TiO_2 particles is 3.85 g/cm^3 and then the density of rutile-TiO_2 after HEBM is changed to be about 3.55 g/cm^3, which is decreased about 15% compared with 4.20 g/cm^3 for initial rutile-TiO_2 state.

Figures 3(a) and 3(b) show that both O 1s and Ti 2p of XPS binding energy spectra for rutile-TiO_2 particles move towards high energy after HEBM process. The increase of O 1s binding energy is considered to be the contribution of oxygen vacancy, while the increase of that for Ti 2p is attributed to structural change and defect accumulation.[30] That literatures reported Ti^{3+} appeared in TiO_2 particles after treatment of HEBM,[30,31] is not observed by us. This may be due to the small size of TiO_2 nanoparticls, and Ti^{3+} is easy to be oxidized into Ti^{4+} in the air.

Although many reports have mentioned that HEBM can produce a large number of oxygen vacancies in particles,[28–32] it is still a challenge to observe oxygen vacancies directly and detect their concentration. Electron paramagnetic resonance (EPR) detection was performed on a sample to determine whether oxygen vacancies appeared in TiO_2 particles after HEBM. Figure 3(c) compares the change of g factor of EPR for TiO_2 particles before and after HEBM process. $g = 2.003$ can be observed in milled TiO_2 particles, which is EPR characteristic structure of oxygen vacancy capturing an electron, while $g = 2.000$ for unmilled TiO_2 particles, which may be the contribution of free radicals or free electrons.[30,33]

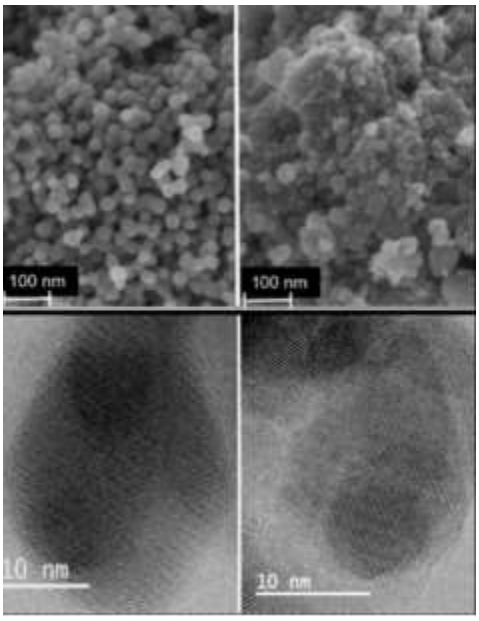

Fig. 1. STEM (top) and HRTEM (bottom) images of TiO_2 nanoparticles before (left) and after (right) HEBM.

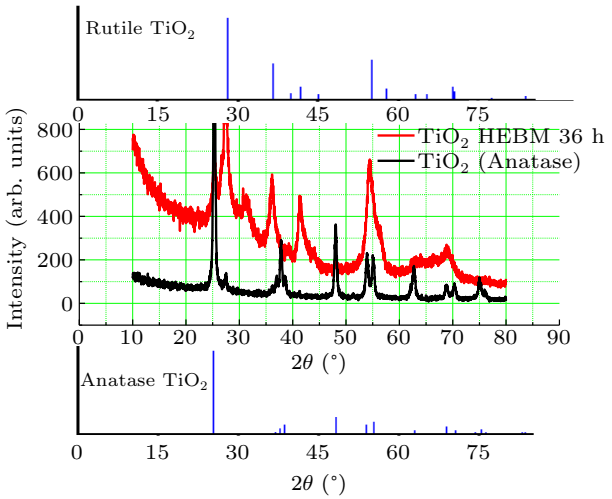

Fig. 2. XRD patterns of anatase structure TiO_2 powder before (black) and after (red) HEBM. The upper and lower are rutile and anatase TiO_2 powder diffraction standards, respectively.

The XAFS technique can study the atomic neighbor structure and is an effective method for studying oxygen vacancies quantitatively by analyzing the change of coordination number. We have applied the XAFS method to study the near neighbor structure of Ti atoms in TiO_2 particles before and after HEBM and then the oxygen vacancy content has been obtained by analyzing the change of coordination number of O atoms surround Ti atoms. For example, after 52 hours of

HEBM, the average coordination number of Ti–O atoms decreases from 6 to 4.8, and then we can know that oxygen vacancies account for about 20% of the total O atoms. The investigations of XAFS for TiO_2 particles by HEBM under different conditions show that the oxygen vacancy accounts for about 10%–20% and even more of the total O atom number depending on the period of HEBM. Detailed results of the XAFS analysis will be reported in a separate paper.

All these indicate that HEBM causes a large number of defects such as oxygen vacancies created in TiO_2 nanoparticles, of which the structure is changed from anatase to rutile. TiO_2 is a kind of non-stoichiometric compound expressed as TiO_{2-X} with X in a wider range.[33–37] According to our XAFS analysis, oxygen vacancies account for about 10%–20% of the total oxygen atoms. The density measurements show that the density of TiO_2 particles decreased by 15% after HEBM, which should be caused by a large number of grain boundary defects and oxygen vacancies in the particles. The existence of these oxygen vacancies in TiO_2 particles is the key factor to produce ID-ER effect.

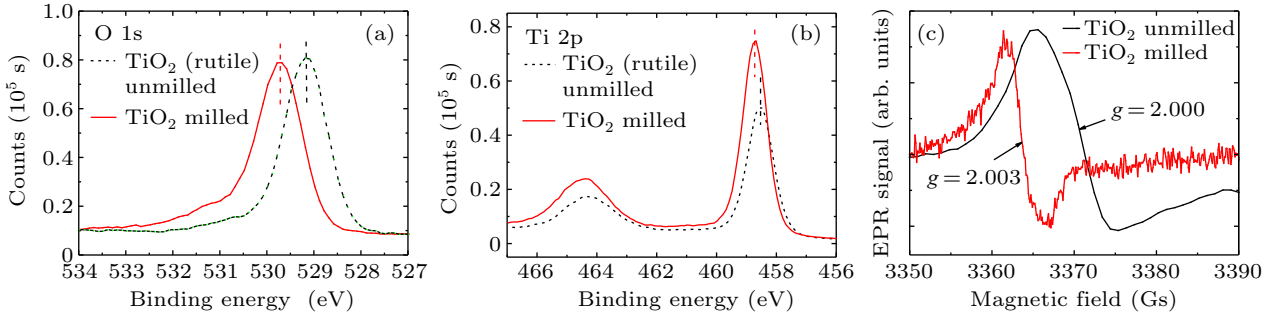

Fig. 3. XPS spectra of O 1s (a) and Ti 2p (b) of rutile-TiO_2 particles before and after HEBM. (c) The change of g factor of EPR for TiO_2 particles before and after HEBM, the unit 1 Gs = 10^{-4} T.

3.2. Yield stress of ID-ER fluids

The ER fluids consisted of the particles treated by HEBM to contain oxygen vacancies or conductive microclusters exhibit strong ER effect with yield stress up to several hundred kPa. In turn, the yield stress of the ER fluid made of unmilled TiO_2 particles is very low reaching only few kPa even for a sample with high volume fraction. In the following, the yield stress of two ID-GER fluids, vacancy type, and conducting microcluster type, varying with the electric field are given, respectively, while the latter is only described briefly.

(i) Vacancy-type ID-ER fluid

Figure 4(a) shows the relationship of yield stress τ_y and current density ρ varying with electric field E of ID-ER fluid, which was fabricated by mixing the TiO_2 particles containing oxygen vacancies to 32# machine oil with a volume fraction of $\phi = 43\%$. Because the yield stress was not very high, the slip effect of plate surface in the measurement can be negligible and then the measured values should truly reflect the relation between τ_y and E. In this case τ_y–E curve can be well fitted by $\tau_y = a + bE^2$, showing the relation $\tau_y \propto E^2$. In contrast, for an ID-ER fluid with $\phi = 54\%$ shown in the inset of Fig. 4(a), the yield stress is high and some skid on the electrode plate was observed during measuring. The slippage results in the measured yield stress being lower than the actual value in the region of higher yield stress values deviating apparently from $\tau_y \propto E^2$ relation. The principle of the relation of τ_y *versus* E will be discussed later. The relationship between the yield stress τ_y and the volume fraction ϕ of ID-ER fluids made by mixing the TiO_2 particles with 32# machine oil and 10# silicon oil are shown in Fig. 4(b) respectively.

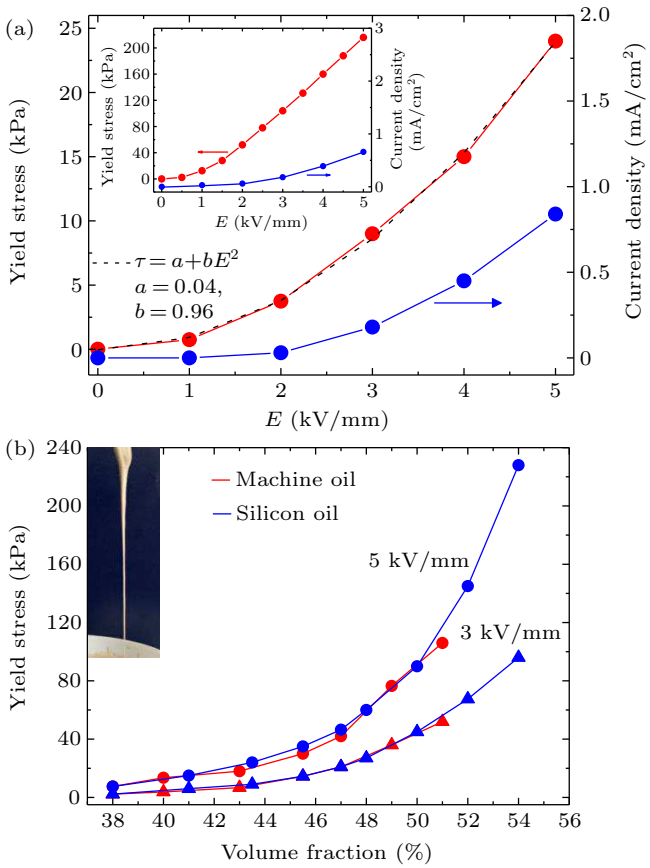

Fig. 4. (a) The dependence of τ_y and ρ on E of ID-ER fluid with $\phi = 43\%$, which can be fitted by $\tau_y = a + bE^2$ with $a = 0.04$ and $b = 0.96$. Inset is the τ_y–E curve for $\phi = 54\%$. (b) The relation of τ_y *versus* ϕ for the ID-ER fluids consisted of HEBM milled TiO_2 nanoparticles and 10# silicone oil or 32# machine oil at 3 kV/mm and 5 kV/mm respectively. Inset is the photo of ID-ER sample with $\phi = 54\%$.

As seen in Fig. 4(b) that τ_y of ID-ER fluid can reach more than 200 kPa as the volume fraction is higher, and the sample still shows good fluidity. The leakage current density as low as less than 20 μA/cm^2 under a field of 5 kV/mm either by using silicon oil or machine oil. When preparing with silicone oil, because of its good temperature stability, the yield stress is almost unchanged in the range of 0 °C–100 °C, while it will change about 10% in machine oil. In addition, these ER fluids have good settlement resistance, and no obvious settlement has been observed in the sample placed for several months.

The yield stresses of the ER fluids prepared with HEBM treated rutile-TiO_2, $BaTiO_3$, $CaTiO_3$, $CaCu_3Ti_4O_{12}$, LiB_3O_5, Al_2O_3, and SiO_2 particles are shown in Fig. 5 respectively. All of them show good ER behavior except for SiO_2 particles. The low yield stress of ER fluid containing milled SiO_2 particles is due to the low dielectric constant of SiO_2 causing the inability for forming a high local electric field between particles.

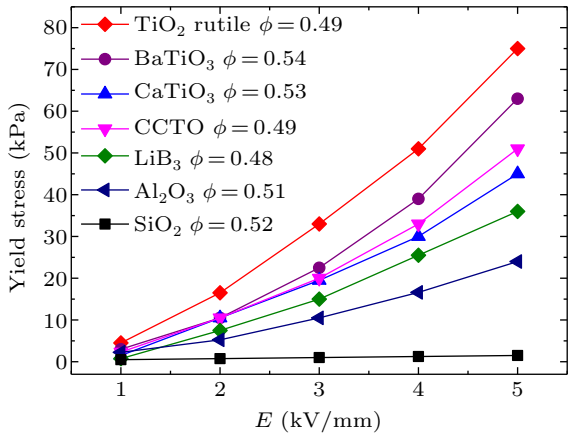

Fig. 5. Relationship between the yield stress and electric field of ID-ER fluids prepared respectively by rutile-TiO_2, $BaTiO_3$, $CaTiO_3$, $CaCu_3Ti_4O_{12}$ (CCTO), LiB_3O_5, Al_2O_3, SiO_2 particles treated by HEBM.

(ii) Conductive microcluster type ID-ER fluid

In our previous report, TiO_2 particles inlaid with carbon microclusters were obtained by heating the Ti–O powder, which were originally made from wet chemistry, and the prepared ER fluid with these TiO_2 particles showed giant ER effect.[23] It is more convenient to prepare dielectric particles inlaid with conductive microclusters by HEBM technique, especially to disperse metal microclusters in the dielectric particles. For example, by mixing small amount graphite (0.67 wt%), Au (3 wt%), Ni (2 wt%) or stainless steel (6 wt%) powders to anatase-TiO_2 particles respectively to process by HEBM, the ER fluids composed with those particles perform good GER effects (*i.e.*, conductive microcluster-type ID-ER fluids) as shown in Fig. 6. The proportion of conductive microclusters embedded in the particles is low, no obvious effect on current density is able to be observed.

In order to confirm the formation of conductor microclusters in TiO_2 particles by mixed small amount of conductors, the near neighbor structures of Ni and Au contained in TiO_2 has been analyzed by XAFS technique, respectively. The results show that Ni atoms are mostly oxidized with Ni–O coordination and only a small handful of Ni atoms form Ni–Ni coordination being dispersed in TiO_2 particles with the form of metal microclusters. Au atoms are not easy to be oxidized, and all of them form Au microclusters dispersed in TiO_2 particles keeping the particles being gray color. Some other easily oxidized metals, such as Al, Ti, Zn, and Cu, were mixed into TiO_2 to perform HEBM. All these metals were oxidized in HEBM process, or gradually oxidize after being placed in the air and then the color of TiO_2 particles became lighter. For example, XAFS analysis for TiO_2 particles mixed with 2-wt% Cu after HEBM treatment shows that there is only Cu–O coordination without Cu–Cu nearest neighbor existed. This indicates that the metal Cu atoms in TiO_2 particles after HEBM all are oxidized and there are no Cu metal microclusters. Detailed results of the above XAFS measurements and analyses will also be published separately.

It should be pointed out that TiO_2 particles embedded into metal microclusters by HEBM also contain oxygen vacancies, and these oxygen vacancies will contribute to the ID-ER effect as well. However, the HEBM period required to inlaid metal microclusters to the particles is shorter.

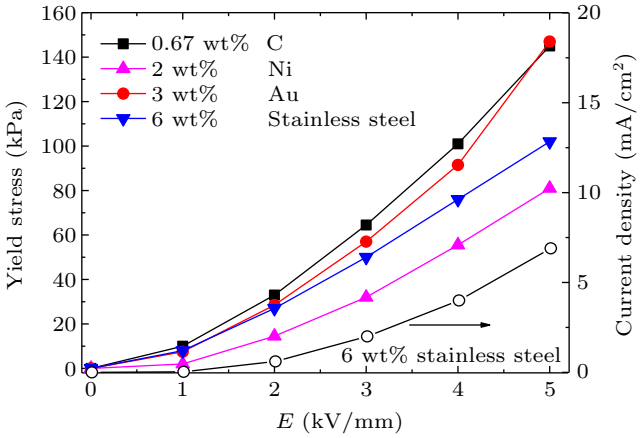

Fig. 6. The relationship between yield stress and E of ID-ER fluid consisted of TiO_2 particles containing graphite, Au, Ni, and stainless steel microclusters, respectively. The volume fractions of particles in ER fluids are about 50%.

3.3. Dynamic response of shear stress to electric field *E(t)* for ID-ER fluid

The response time of the shear stress to applied electric field $E(t)$ for ER fluids is an important indicator of their performance. We have studied the response behaviors of ID-ER fluid in square $E(t)$ field and in sinusoidal $E(t)$ field, respectively, as shown in Figs. 7 and 8. The ID-ER sample was composed of TiO_2 particles with oxygen vacancies contained and machine oil ($\phi \approx 48\%$).

Figure 7(a) shows a typical graph of shear stress varying with a square wave $E(t)$ ($E_{\max} = 4$ kV/mm) at shear rate $\dot{\gamma} = 120$ s^{-1} while figure 7(b) is the enlarged view in the region of

a single $E(t)$ pulse of Fig. 7(a). Figures 7(c) and 7(d) respectively show the responses of normalized shear stress at front edge and back edge of square $E(t)$ field ($E_{\max} = 3$ kV/mm) at different shear rate $\dot{\gamma}$. The delay time is defined by using the width at half maximum of the stress change and denoted as $t_{\text{half}}^{\text{front}}$ and $t_{\text{half}}^{\text{back}}$ for front edge and back edge, respectively. It can be seen that $t_{\text{half}}^{\text{front}}$ decreases with the increase of shear rate and is about 4 ms as $\dot{\gamma} \geq 20\ \text{s}^{-1}$. While $t_{\text{half}}^{\text{back}}$ at back edge is larger than $t_{\text{half}}^{\text{front}}$ and increases with $\dot{\gamma}$ slightly, tending to a value about less than 20 ms. It means that the response time of the ID-ER fluid is shorter at the front edge of a square wave $E(t)$ and longer at the back edge. The changes of $t_{\text{half}}^{\text{front}}$ and $t_{\text{half}}^{\text{back}}$ with shear rate $\dot{\gamma}$ are illustrated in the insets of Figs. 7(c) and 7(d), in which the colors of the data points correspond to that of each shear stress curve, respectively.

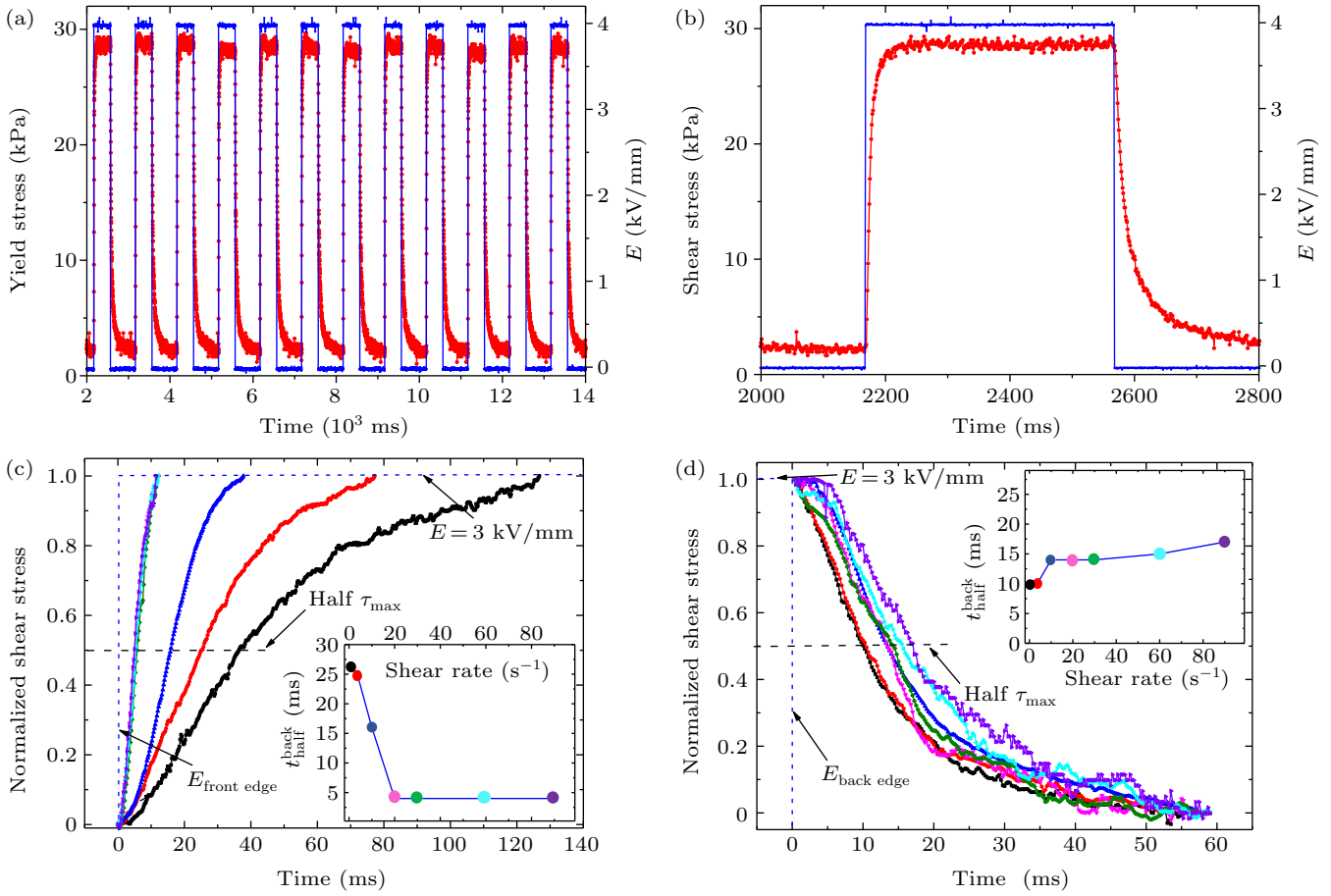

Fig. 7. Response behavior of the shear stress to square wave $E(t)$. (a) Response of shear stress to a square wave $E(t)$ of $E_{\max} = 4$ kV/mm and frequency $f = 1$ Hz (blue dash line), of which the pulse width is 400 ms and the sampling rate is 1000 s^{-1} at $\dot{\gamma} = 120\ \text{s}^{-1}$. (b) Enlarged view of (a) for a single $E(t)$ pulse. Panels (c) and (d) respectively show the normalized shear stresses at front edge and back edge of square wave $E(t)$ for different shear rates $\dot{\gamma}$, where $E_{\max} = 3$ kV/mm (blue dotted line), $f = 1$ Hz and sampling rate is 4000 s^{-1}. The insets of panels (c) and (d) show the changes of $t_{\text{half}}^{\text{front}}$ and $t_{\text{half}}^{\text{back}}$ with $\dot{\gamma}$, respectively.

The reasons for the relationship of response time $t_{\text{half}}^{\text{front}}$ and $t_{\text{half}}^{\text{back}}$ with $\dot{\gamma}$ can be explained as follows. The electric polarization response is very fast and its contribution to relaxation time is negligible. Under the action of electric field, particle motion and configuration refactoring occur during shearing, resulting in the adjustment of force among all particles to cause the shear stress changing. Therefore, the correlation between shear rate and response time must be caused by the effect of shear motion on particle configuration. It was observed that the lamellar structures called shear bands can formed in ER fluids under electric field applied and shear action.[38,39] The higher the shear rate, the wider the shear bands. At the start edge of $E_{\max}$, a slightly higher shear rate is conducive to particle movement and promotes the formation of layered structures, which results in a shorter response time, as shown in Fig. 7(c). However, the high shear rate has caused the existence of a wide shear band in the ER fluid as $E(t) = E_{\max}$. When $E(t) \to 0$, it should take a long time for the structure to recover from the wide shear band to the uniform initial state and thus $t_{\text{half}}^{\text{back}}$ should be slightly longer at higher shear rates, as illustrated in Fig. 7(d). In the case of high shear rate, the configuration changes already are fast, and then the response time is not sensitive to the shear rate as showing in the insets of Figs. 7(c) and 7(d).

The response behaviors of ID-ER fluid in sinusoidal $E(t)$ field from $f = 1$ Hz to 100 Hz were measured at $\dot{\gamma} = 50\ \text{s}^{-1}$

and selected plots for $f = 1$ Hz, 5 Hz, and 50 Hz are shown in Figs. 8(a)–8(c), respectively. It can be seen that with the increase of frequency, the distortion and delay of shear stress become serious, resulting in the amplitudes of shear stress decreasing with the increase of frequency. The maximum values τ_{max} and minimum τ_{min} of shear stress in sinusoidal fields from 1 Hz to 100 Hz are shown in Fig. 8(d). For a comparison, the inset of Fig. 8(d) shows the variation of τ_{max} and τ_{min} with the frequency for PM-ER fluid.[40]

The above results indicate that the delay of shear stress in square $E(t)$ field leads to the shear stress in sine wave $E(t)$ field decreasing with the increase of frequency f. The amplitude of shear stress reduces by about 50% as $f = 50$ Hz. However, compared with that in PM-ER liquid,[40,41] there is a significant improvement.

In addition to the shear rate discussed above, the response of the shear stress of the ER to the electric field is also related to many other factors, such as volume fraction, electric field strength, oil viscosity, particle density and size, and the design of the ER device.

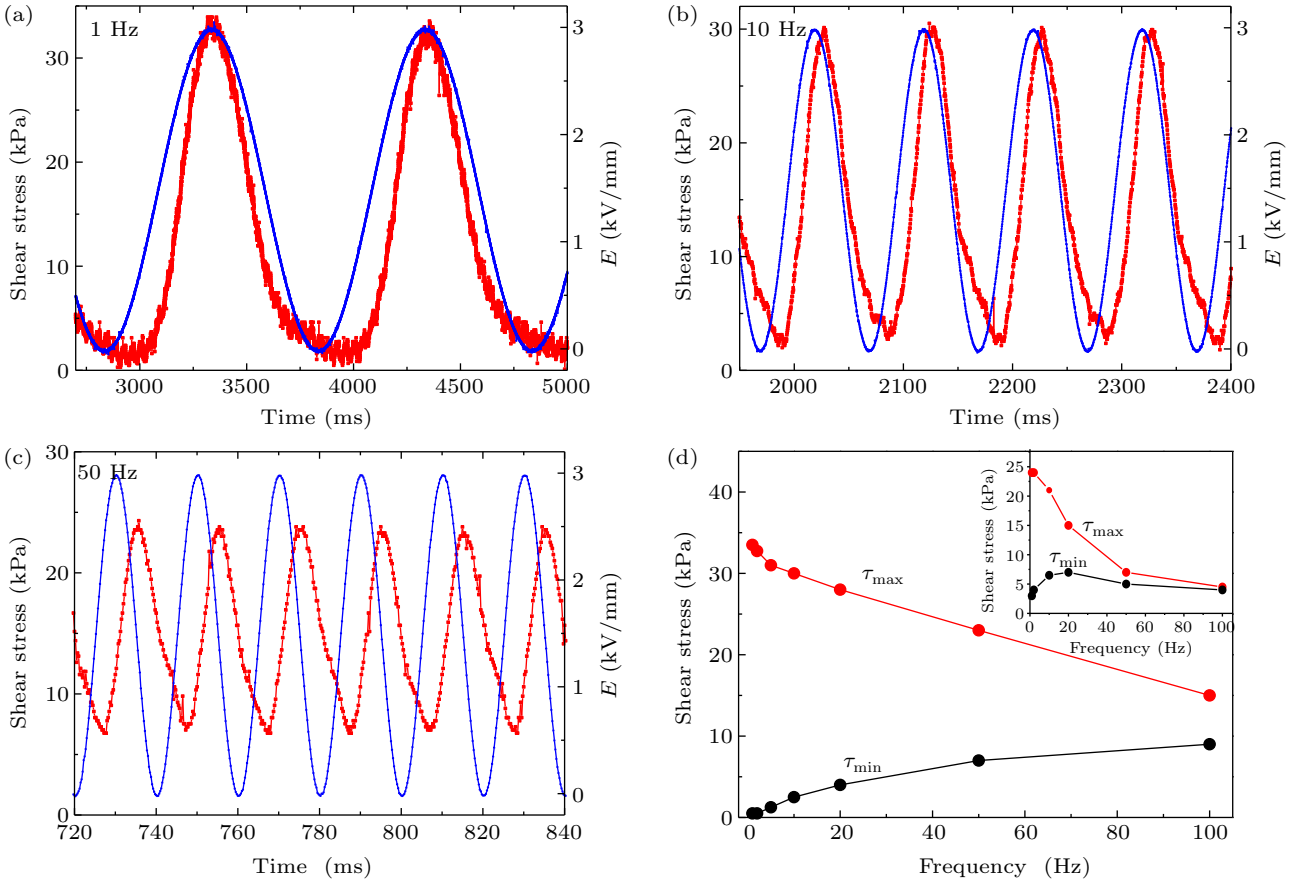

Fig. 8. Response of shear stress (red) with sinusoidal waves $E(t)$ (blue) of $E_{max} = 3$ kV/mm at different frequencies, shear rate $\dot{\gamma} = 50$ s^{-1}, sampling rate 4000 s^{-1}. Panels (a)–(c) show the relationship between shear stress and sinusoidal $E(t)$ for $f = 1$ Hz, 10 Hz, 50 Hz, respectively. (d) The variation of τ_{max} and τ_{min} with f, inset shows the behavior of PM-ER fluids.

3.4. Wear resistance

The wear resistance of ER fluid is also an important indicator for their applications. Although PM-ER fluid can achieve high shear stress, the serious disadvantage is that the coated or modified layers on the particle surfaces are easy to wear and fall off, making its shear stress constantly reducing with service time. So that PM-ER fluid is also not suitable to be put into application.[20,21] In order to test the service life of ID-ER fluids, three different ER samples composed of TiO_2 particles treated by HEBM were used for wear resistance test, respectively. The samples were placed in sealed rotary cylinder, as illustrated in inset of Fig. 9, to carry out friction test with a shear rate 300 s^{-1} without electric field applied and were rubbed for 240 h, 340 h, and 140 h respectively. During the period, ER samples were taken out several times for measuring the yield stress under applied electric field, and the results are shown by three cases (A), (B), and (C) in Fig. 9 with red symbols. Where, case (A) is the yield stress for a conductive microcluster-type ID-ER fluid composed of TiO_2 particles containing 3-wt% stainless steel, cases (B) and (C) are for vacancy-type ID-ER fluids. The results show that the yield stresses of these ID-ER fluids are almost unchanged during the test and they have excellent wear resistance. By contrast, the yield stress of PM-ER fluid decreases rapidly with wear time as illustrated by cases (D) and (E) of Fig. 9, represented the PM(S)-ER and PM(L)-ER fluids respectively. Here, PM(S)-

ER was consisted of the solid particles with polar molecules coated while PM(L)-ER fluid was prepared by adding polar molecules to the liquid.

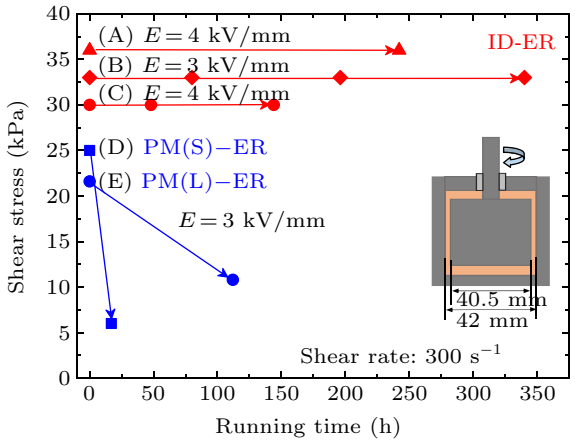

Fig. 9. Wear resistance of ER fluid samples: cases (A), (B), and (C) are the measured values of yield stress for three ID-ER samples during the period of wearing 240 h, 340 h, and 140 h respectively (red color). The blue symbols are the wearing test results of PM-ER sample, where case (D) is PM(S)-ER fluid and case (E) is for PM(L)-ER fluid.

Although the wear life of PM(L)-ER fluid is about five times longer than that of PM(S)-ER fluid,[21] it is still not up to the requirements of practical use. The failure of PM-ER fluid is caused either by the shedding of the polar molecules on the particles due to friction, or due to the loss of their polarities by attracting such as space charges during operation.

It can be seen that ID-ER fluid has advantages of both high shear stress and wear resistance, which breaks through the difficulties that the ER fluid cannot be applied in practice for a long time. Therefore, the ID-ER fluid is expected to be a practical material for ER technology.

3.5. Physical mechanism and related issues of ID-ER effect

HEBM can significantly change the structure and microscopic morphology of TiO_2 nanoparticles, resulting in a large number of oxygen vacancies or embedded conductive microspheres, as shown in Fig. 10(a). As for conductive microsphere-type ID-ER fluid, we have explained the mechanism in earlier publication,[23] and only that of vacancy-type ID-ER fluid will be discussed here.

After passing the HEBM, the oxygen vacancies in TiO_2 particles can capture one or two electrons, or not, which can all be regarded as the local charged centers. Such charge centers, localized in the regions of vacancies, are neither like the tightly bound electrons in atoms, nor like the space charges spreading over a wide area in the medium. Oxygen vacancies can be polarized into induced dipole under an electric field, and their interactions are the source of vacancy type ID-ER effect.

As an electric field E is applied, TiO_2 particles will be polarized and attract each other to get closer. Due to its high dielectric constant, the local electric field E_{loc} in the gap between two particles can be as high as 10^2–10^3 times of E.[15–19,39,42] E_{loc} is nearly proportional to E, and its value is related to particle dielectric constant, particle size, particle spacing, and the position at the gap. E_{loc} can reach about 10^8 V/m to 10^9 V/m, when E is 1×10^6 V/m to 5×10^6 V/m.

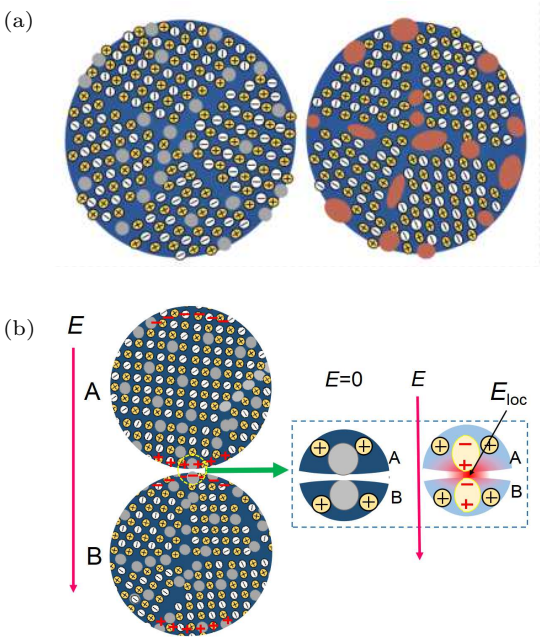

Fig. 10. (a) The internal structure and morphology of nanoparticles after HEBM. The left, the particles contain oxygen vacancies (gray); the right, the conductor microcluster (brown) embedded in the particle. (b) In the case of the particles containing vacancies. The right, an enlarged image shows that E_{loc} at the interval causes the induced dipole interaction from the surfaces of particles A and B.

We can approximately calculate the induced dipole moment and the interaction force at the particle gap. The induced dipole moment μ under the action of E_{loc} can be expressed as $\mu=\alpha E_{loc}$, where α is the polarizability. While α can be calculated by $4\pi\varepsilon_s\varepsilon_0 r^3$,[16,39,43] where ε_s is the dielectric constant of the solid medium, ε_0 is the dielectric constant of the vacuum, and r is the radius of the oxygen vacancy. As $r=0.1$ nm,[44] $\varepsilon_s=100$, $E_{loc}=1\times10^9$ V/m, then $\mu\approx3.34$ Debye with a dipole size of 0.2 nm.

At the gaps between particles, the induced dipole on the surface of particle A can interact with that on the surface of particle B along the direction of the electric field. The force can be approximately expressed as $f_{D-D}=3\mu^2/2\pi\varepsilon_f\varepsilon_0 d_{D-D}^4$,[45] d_{D-D} is the center distance of the two induced dipoles, and ε_f is the dielectric constant of the oil. As $d_{D-D}=0.4$ nm and $\varepsilon_f=2$, then $f_{D-D}\approx1.32\times10^{-10}$ N with a relation of $f_{D-D}\propto\mu^2\propto E^2$. The above estimation is only a rough approximation because the uneven distribution[15,19,42] of E_{loc} is unconsidered.

The interaction force between polarized particles in conventional ER fluid can be estimated roughly according to common method.[15,16] For TiO_2 particles with a radius of 10 nm and an interval of $\delta=0.2$ nm in $E=5\times10^6$ V/m field, the interaction force between two polarized particles is

4.9×10^{-12} N. Obviously, f_{D-D} is more than an order of magnitude larger than the force induced by polarized particles. This can explain why the yield stress of ID-ER fluid is much higher than that of conventional ER fluid.

The above analysis shows that f_{D-D} is proportional to E^2, that is the yield stress τ_y in ID-ER fluid should be proportional to E^2, as shown in Fig. 4(a). This behavior can be also observed in other ID-ER samples as shown in Figs. 5 and 6. This relation of $\tau_y \propto E^2$ of ID-ER fluid is different from that of $\tau_y \propto E$ in PM-ER fluid, in which the polar molecules with intrinsic dipole moment adsorbed on the particle surface are oriented along the E_{loc} direction and the interactions occur, and thus the force $f \propto E$.[9,11,12] On the other hand, the polar molecules adsorbed on the active particle surface in PM-ER fluid only exist on the particle surface and possess low adsorption energy, thus they are easily lost by friction. As shown in Fig. 9, the yield stress of PM-ER fluid is reduced by about half after tens of hours of wear. Meanwhile, ID-ER fluid has good temperature stability, with the change of less than 10% in the temperature range of 25 °C–170 °C,[23] while the shear stress of PM-ER fluid will change by one times or even more in the 0 °C–100 °C range. In addition, the response time and frequency response of ID-ER fluid are improved compared with that of PM-ER fluid, maybe due to the response of induced polarization is faster than the reorientation of polar molecules.

It is difficult to make all HEBM-prepared particles with identical function. For ER fluids with low volume fraction, the particles form chain structures when an electric field is applied. Each chain can contain about 5×10^5 particles with a radius of 10 nm when the electrode plates are spaced 1 mm apart. The failure of individual particle can lead to entire chain ineffective. There may be not a few such failed chains between plates, resulting in too low shear stress for ID-ER fluid with low volume fraction. When the volume fraction reaches about 37% and the particles form network structure in ER suspension,[4] then the influence from these failed particles can be reduced. Therefore, only the ID-ER fluid with higher volume fraction possesses high shear stress, then the zero-field viscosity of the ID-ER fluid prepared by present process is bound to be higher. This shortcoming needs to be further improved through research. For example, the zero-field viscosity of an ID-ER fluid or the stress of it with lower volume fractions can be improved by changing the particle preparation method or changing the dispersion composition. The previous studies in PM-ER fluids have obtained successful results.[46,47]

The vacancy-type ID-ER effect described in the present paper is due to the induced polarization of oxygen vacancies produced by HEBM technique. Can oxygen vacancies, or positive ion vacancies, produced by other methods produce similar effect? In principle, there may be similar results, but further confirmation is needed. Zhao *et al.*[5] reported that doping rare earth or transition metal in oxide powder can enhance the ER effect, which may be caused by the polarization of oxygen vacancies or other defects introduced by doping.

4. Conclusion

The effect of traditional dielectric ER fluids originates from particle polarization interaction, which cannot meet the requirements of applications because of the low yield stress. Later on, the giant ER fluids or saying PM-ER fluids with high shear stress were developed, which were considered promising for application. However, because the particles were prepared by surface coating or modification, the polar molecules adsorbed on the surface of particles are vulnerable to wear and loss of efficacy. So that such PM-ER fluids are also unable to be widely used in practice.

In our study, a new type of giant ER fluid called induced dipole-dominated ER (ID-ER) fluid has been developed. The preparation method, physical principle, and properties are introduced in this paper. Dielectric particles, such as TiO_2, are processed by HEBM to generate a large number of oxygen vacancies or make conductor microclusters embedded in the particles. These oxygen vacancies or conductor microspheres can form induced dipoles in the electric field. Due to the high local electric field E_{loc} between particles, the dipole moment $\mu = \alpha E_{loc}$ of the induced dipole can be large. The interactions of these induced dipoles between adjacent particles are very strong, resulting in the shear stress of the ID-ER fluid up to hundreds of kPa. The above mechanism results in the relationship between the shear stress and the electric field being as $\tau_y \propto E^2$ in ID-ER fluid. The experimental results show that in addition to high shear stress, ID-ER fluid also provides the advantages of low current density, fast response time, long wear resistance, good temperature stability, and anti-sedimentation. Moreover, the preparation method is simple and easy to repeat.

In conclusion, the action principle and preparation method of ID-ER fluid are obviously different from either the dielectric-type ER fluid or the PM-ER fluid. This ID-ER fluid with excellent comprehensive performance should be a new generation of ER fluid suitable for practical applications.

Acknowledgments

Thanks to Wang Qiang, Xu Yanping, Liu Rui, Yu Richeng, Guo Qinlin, Wu Zhonghua, Zhong Jiajun, Duan Ran for their help in experiments, and to Zhou Luwei for his helpful discussion.

Project supported by the National Key Research and Development Program of China (Grant No. 2017YFA0403000) and the National Natural Science Foundation of China (Grant No. 11874430).

References

[1] Winslow W M 1949 *J. Appl. Phys.* **20** 1137
[2] Davis L C 1992 *Appl. Phys. Lett.* **60** 319
[3] Tao R and Jiang Q 1994 *Phys. Rev. Lett.* **73** 205
[4] Hao T 2002 *Adv. Colloid Interface Sci.* **97** 1
[5] Zhao X P and Yin J B 2011 *Smart Soft Materials Turned by Electric Field* (Beijing: Science Press) (in Chinese)
[6] Ma H R, Wen W J, Tam W Y and Sheng P 1996 *Phys. Rev. Lett.* **77** 2499
[7] Zhang Y L, Ma Y, Lan Y C, Lu K Q and Liu W 1998 *Appl Phys Lett.* **73** 1326
[8] Zhang Y L, Lu K Q, Rao G H, Tian Y, Zhang S H and Liang J K 2002 *Appl Phys. Lett.* **80** 888
[9] Wen W J, Huang X, Yang S, Lu K Q and Sheng P 2003 *Nat. Mater.* **2** 727
[10] Yin J B and Zhao X P 2004 *Chem. Phys. Lett.* **398** 393
[11] Lu K Q, Shen R, Wang X Z, Sun G, Wen W J and Liu J X 2006 *Chin. Phys.* **15** 2476
[12] Xu L, Tian W J, Wu X F, Cao J G, Zhou L W, Huang J P and Gu G Q 2008 *J. Mater. Res.* **23** 409
[13] Shen R, Wang X Z, Lu Y, Wang D, Sun G, Cao Z X and Lu K Q 2009 *Adv. Mater.* **21** 4631
[14] Orellana C S, He J B and Jaeger H M 2011 *Soft Matter* **7** 8023
[15] Davis L C 1997 *J. Appl. Phys.* **81** 1985
[16] Tao R J, Jiang Q and Sim H K 1995 *Phys. Rev. E* **52** 2727
[17] Gonon P, Foulc J, Atten P and Boissy C 1999 *J. Appl. Phys.* **86** 7160
[18] Tan P, Tian W J, Wu X F, Huang J Y, Zhou L W and Huang J P 2009 *J. Phys. Chem. B* **113** 9092
[19] Jiao M C 2011 PhD thesis, Institute of Physics, Chinese Academy of Sciences (in Chinese)
[20] Wu X F, Zhou L W and Huang J P 2009 *Eur. Phys. J. Appl. Phys.* **48** 31301
[21] Lu K Q and Shen R 2017 *Smart Mater. Struct.* **26** 054005
[22] Shen R and Lu K Q *Chinese invention patents:* ZL 2022 1 0303339.3 and ZL 2022 1 0301781.2
[23] Qiu Z H, Shen R, Huang J, Lu K Q and Xiong X M 2019 *J. Mater. Chem. C* **7** 5816
[24] Benjamin J S and Volin T E 1974 *Metallurgical and Materials Transactions B* **5** 1929
[25] Suryanarayana C and Nasser Al-Aqeeli 2013 *Progress in Materials Science* **58** 383
[26] Zhu X K, Lin Q S, Chen T L, Cheng B C and Cao J C 1999 *Powder Metallurgy Technology* **17** 291
[27] El-Eskandarany M S 2001 *Mechanical Alloying for Fabrication of Advanced Engineering Materials* (New York: William Andrew Publishing, Inc.)
[28] Begin-Colin S, Girot T, Mocellin A, Caer G L 1999 *Nanostructured Materials* **12** 195
[29] Pan X Y 2004 PhD thesis, Shanghai University (in Chinese)
[30] Rinaudo M G, Beltran A M, Fernandez M A, Cadús L E and Morales M R 2020 *Materials Today Chemistry* **17** 100340
[31] Indris S, Amade R, Heitjans P, Finger M, Haeger A, Hesse D, Grunert W, Borger A and Beck K D 2005 *J. Phys. Chem. B* **109** 23274
[32] Zhang B Q, Lu L and Lai M O 2003 *Physica B* **325** 120
[33] Micic O I, Zhang Y N, Cromack K R, Trifunac A D and Thurnauer M C 1993 *J. Phys. Chem.* **97** 7277
[34] Banakh O, Schmid P E, Sanjines R and Levy F 2002 *Surface and Coatings Technology* **151–152** 272
[35] Li Z Q, Hu R, G J, Ru L Y and Wang H H 2012 *Mater. Sci. Tech.* **20** 80
[36] Hou Q Y, Uyun G and Zhao C W 2013 *Acta Phys. Sin.* **62** 167201 (in Chinese)
[37] Wang Q, Zhang S, He H N, Xie C L, Tang Y G, He C X, Shao M H and Wang H Y 2021 *Chem. Asian J.* **16** 19
[38] Tang X, Li W H, Wang X J and Zhang P Q 1999 *Int. J. Mod. Phys. B* **13** 1806
[39] Zhou L W 2019 *Introduction to Soft Matter Physics* (Singapore: World Scientific Publishing Co. Ltd.)
[40] Shen R, Liu R, Wang D, Chen K, Sun G and Lu K Q 2014 *RSC Adv.* **4** 61968
[41] Zhao H Q, Shen R and Lu K Q 2018 *Chin. Phys. B* **27** 078301
[42] Jiao M C, Sun G, Wang Q and Lu K Q 2012 *Mod. Phys. Lett. B* **26** 1150007
[43] Sun M Z 2000 *Fundamentals of Dielectric Physics* (Shenzhen: South China University of Technology Press) (in Chinese)
[44] Zhao L, Blanka M K and Yoshio N 2017 *Phys. Rev. B* **95** 054104
[45] Israelachvili J N 2000 *Intermolecule and Surface Force* (London: Academic)
[46] Wu J H, Song Z Y, Liu F H, Guo J J, Cheng Y C, Ma S Q and Xu G J 2016 *NPG Asia Mater.* **8** e322
[47] Liang Y D, Yuan X, Wang L J, Zhou X F, Ren X J, Huang Y F, Zhang M Y, Wu J B and Wen W J 2020 *Colloid and Interface Science* **564** 381